Metaheuristic Algorithms with Applications

www.maa.reapress.com

Metaheur. Algor. Appl. Vol. 1, No. 3 (2024) 208–226.

Paper Type: Original Article

On Decreasing Mismatch-Induced Stresses in a Heterostructure by Preliminary Radiation Processing of the Substrate

Evgeny. L. Pankratov*

Nizhny Novgorod State Agrotechnological University, 97 Gagarin Avenue, Nizhny Novgorod, 603950, Russia; elp2004@mail.ru.

Citation:

Received: 17 April 2024 *Revised: 02 June 2024* *Accepted: 19 August 2024*	Pankratov, E. L. (2024). On decreasing mismatch-induced stresses in a heterostructure by preliminary radiation processing of the substrate. *Metaheuristic algorithms with applications, 1*(3), 208-226.

Abstract

The continuous miniaturisation of solid-state devices and the proliferation of multilayer heterostructures in modern microelectronics, optoelectronics, and power electronics have placed epitaxial-layer quality at the centre of device-engineering research. A persistent obstacle in these systems is the lattice- and thermo-elastic mismatch between the substrate and the epitaxial layer, which gives rise to mismatch-induced stresses that degrade crystalline quality, generate threading dislocations, and ultimately limit device yield [1–3]. This article introduces and elaborates an approach aimed at decreasing mismatch-induced stresses in a heterostructure by subjecting the substrate to preliminary radiation processing before the gas-phase epitaxial growth of the active layer. The damaged near-surface region created by ionising radiation acts as a sacrificial defect reservoir whose recombination and accelerated diffusion during high-temperature Vapour-Phase Epitaxy (VPE) modify the local chemical potential and, in turn, the elastic state of the growing interface. To describe this coupled mass-and-heat-transfer problem, the present work develops an analytical framework based on the Method of Averaging of Function Corrections (MAFC), originally introduced by People and Bean [4]. The framework simultaneously accommodates spatial and temporal variations of the transport coefficients, the nonlinearity of the recombination kinetics of point defects and their complexes, and the coupling between the elastic, diffusive, and hydrodynamic fields. Approximate closed-form solutions are obtained to the second order of the MAFC iteration. The analysis indicates that preliminary radiation processing of the substrate may reduce the magnitude of the mismatch-induced stress by approximately 10–30 % for typical VPE conditions and simultaneously smooth the interface between the substrate and the epitaxial layer. The assumptions, the order of accuracy of the iteration, and the principal limitations of the framework are discussed in detail.

Keywords: Heterostructure, Mismatch-induced stress, Radiation processing of substrate, Vapour-phase epitaxy, Method of averaging of function corrections, Mass and heat transfer.

Corresponding Author: elp2004@mail.ru

https://doi.org/10.48313/maa.v1i3.93

1 | Introduction

Multilayer heterostructures form the structural backbone of nearly every active device in contemporary solid-state electronics. Heterojunction bipolar transistors, high-electron-mobility transistors, multi-quantum-well lasers, light-emitting diodes, and modern power diodes all rely on the controlled stacking of epitaxial layers whose bandgap, lattice constant, and thermal expansion coefficient are deliberately varied across the stack [1], [5]. The performance of these devices is governed not only by the bulk transport properties of each layer but also, and often more decisively, by the structural quality of the interfaces between them. As a result, the growth and post-growth engineering of epitaxial heterostructures has become one of the central topics in materials science and device engineering. Recent reviews on GaN-on-SiC, AlGaN/GaN, and III-V multilayer systems consistently highlight interface quality as the dominant factor in device reliability [6–8].

Three families of growth techniques currently dominate the manufacture of epitaxial heterostructures: Molecular Beam Epitaxy (MBE), Vapour-Phase Epitaxy (VPE), including its hydride and organometallic variants, Hydride Vapour-Phase Epitaxy (HVPE) and Metal-Organic Vapour-Phase Epitaxy (MOVPE), and magnetron sputtering. Each technique offers distinct compromises between throughput, interface abruptness, and process temperature. VPE, in particular, has retained a leading role in high-volume manufacturing because it combines reasonably high growth rates with accurate compositional control and the ability to process multiple wafers simultaneously in a single reactor [2], [9], [10]. Modern Computational Fluid Dynamics (CFD) studies of HVPE reactors have shown that careful geometric design of the chamber, particularly the slope and rotation of the substrate holder, can substantially improve the uniformity of the deposited layer and the controllability of the mass transport of reagent species [11–13]. Despite these advances, VPE-grown heterostructures still suffer from a fundamental limitation: the epitaxial layer is rarely lattice-matched to the substrate, so that the as-grown stack carries an intrinsic elastic strain.

The origin of this strain is well understood. When two crystalline solids with different equilibrium lattice constants are joined at a coherent interface, the atomic planes close to the interface deform so that a common in-plane lattice parameter is established across the boundary. The associated elastic energy, proportional to the square of the mismatch parameter, is stored in the heterostructure until it relaxes either plastically, through the nucleation of misfit and threading dislocations, or chemically, through interdiffusion and interfacial reactions [2], [14]. Both relaxation channels degrade the electronic properties of the device: dislocations introduce mid-gap states and act as non-radiative recombination centres, while interdiffusion broadens the nominally abrupt interfaces on which device operation depends. Mitigating mismatch-induced stress is therefore a prerequisite for obtaining epitaxial layers of sufficient quality for advanced device applications.

Several engineering strategies have been developed over the past decades to address this problem. They include the use of graded buffer layers [4], [15], the introduction of compliant or porous substrates, the optimisation of the V/III ratio during growth, the use of low-temperature nucleation layers, and post-growth thermal annealing. Each approach modifies a different aspect of the stress-generation mechanism, and each carries its own limitations in terms of added process complexity, residual defect density, or thermal budget. Recent work on Ar-ion implantation pretreatment of sapphire substrates has demonstrated a reduction of the total dislocation density in GaN epitaxial layers by as much as 65 %, illustrating the practical potential of substrate-oriented defect engineering [16]. The present article pursues an alternative and complementary route, namely the preliminary radiation processing of the substrate before the start of the epitaxial growth.

The underlying physical idea is that a controlled population of point defects introduced into the substrate by ionising radiation serves as a sacrificial defect reservoir. During the subsequent high-temperature VPE process, these defects recombine and diffuse out of the damaged region; their redistribution modifies the local chemical potential of the substrate near the interface and, through the elastodiffusive coupling, the stress state of the growing epitaxial layer.

The objectives of the present work are threefold. First, we develop a coupled analytical model that describes, in a unified framework, the generation, recombination, and diffusion of radiation-induced point defects in the substrate, the elastic response of the heterostructure, and the heat-and-mass transfer that takes place in the VPE reactor. Second, we apply the Method of Averaging of Function Corrections (MAFC), originally introduced by Sokolov [17] and developed in subsequent work [18–20], to obtain approximate closed-form solutions to the resulting nonlinear boundary-value problem. The MAFC has been shown to provide an efficient trade-off between accuracy and analytical transparency for nonlinear transport problems; alternative iterative and stochastic optimisation techniques have also been used in adjacent fields for parameter identification and model reduction [21–27]. Third, we analyse the implications of the solutions for the reduction of mismatch-induced stress and for the smoothing of the epitaxial interface. The thesis of the article is that preliminary radiation processing of the substrate, when combined with the high-temperature environment of VPE, may simultaneously reduce the magnitude of the mismatch-induced stress and improve the morphological quality of the interface provided that the radiation dose and the growth parameters are jointly optimised.

The remainder of the article is organised as follows. The section titled Background and Theoretical Context reviews the physical and historical setting of the problem and defines the scope of the analysis. The Mathematical Model section introduces the geometry of the heterostructure–reactor system, the mass-transfer equations for radiation-induced point defects, the elastodiffusive coupling, and the heat-transfer and gas-dynamic equations. The Methodology section describes the MAFC framework and derives the first- and second-order approximations of the unknown fields. The Results section presents the principal findings and their physical interpretation. The Discussion section elaborates on the broader implications of the findings. The Limitations and Counterarguments section critically reviews the assumptions and competing approaches. The Conclusion synthesises the main findings and offers an outlook on future research directions.

2 | Background and Theoretical Context

2.1 | Heterostructures and the Origin of Mismatch-Induced Stress

A heterostructure is, in its broadest sense, any stack of solid layers in which at least one material parameter chemical composition, crystal structure, doping, or orientation varies along the growth direction. In modern device engineering, the term is most often reserved for epitaxial stacks in which each layer is a single crystal that is crystallographically registered with its neighbour. The coherent registration of two layers with different equilibrium lattice constants, a_s (substrate) and a_EL (epitaxial layer), is parameterised by the mismatch parameter:

$$\varepsilon_0 = (a\_s - a\_EL) / a\_EL, \qquad (1)$$

which quantifies the in-plane strain that must be accommodated by elastic deformation of one or both layers. When $|\varepsilon_0|$ is sufficiently small and the epitaxial layer is sufficiently thin, the strain is stored elastically, and the interface remains coherent. Beyond a critical thickness, first analysed by Matthews and Blakeslee [14] and later refined by People and Bean [4], the stored elastic energy exceeds the line energy of a misfit dislocation, and plastic relaxation sets in [28]. The dislocations nucleated at the interface thread through the epitaxial layer, where they degrade carrier mobility, increase leakage currents, and reduce the radiative efficiency of optoelectronic devices. Recent synchrotron X-ray diffraction and Raman mapping studies on GaN-on-Si epitaxial layers have directly correlated residual stress with threading-dislocation density and have quantified the contribution of superlattice buffers to stress relaxation [29], [30].

Beyond the purely geometrical contribution associated with ε_0, the stress state of an epitaxial stack is also influenced by the difference in thermal expansion coefficients between the substrate and the layer. VPE is carried out at elevated temperatures, typically between 600 °C and 1100 °C depending on the material system. On cooling from the growth temperature to room temperature, the differential thermal contraction introduces an additional thermo-elastic stress that adds to the lattice-mismatch contribution [15], [31]. The total stress at the operating temperature of the device is therefore the superposition of a growth-temperature mismatch component and a thermo-elastic component accumulated during cooling. The two contributions may have opposite signs, so that a layer which is compressively strained at the growth temperature may end up in tension at room temperature, or vice versa, a fact that complicates the design of strain-engineered heterostructures and is exploited, for example, in step-graded AlGaN buffers for GaN-on-SiC technology [7], [15].

2.2 | Radiation Processing of Semiconductors

The interaction of ionising radiation with semiconductor crystals has been studied intensively since the 1950s and is the subject of several authoritative monographs [32], [33]. When energetic particles electrons, ions, or photons impinge on a crystalline solid, they transfer energy to the lattice through a cascade of elastic and inelastic collisions. If the energy transferred to a lattice atom exceeds the displacement threshold, the atom leaves its site and a Frenkel pair is created, consisting of a vacancy and an interstitial. The primary point defects subsequently migrate, recombine, and aggregate into more complex defect structures: divacancies, diinterstitials, and larger clusters. The kinetics of these processes are governed by the local temperature, the local stress state, and the concentrations of the interacting species. Recent reviews have emphasised the multiscale nature of the problem, linking ab-initio defect energetics, kinetic Monte Carlo simulations, and continuum rate-equation models into a unified description of point-defect kinetics [34–36].

Radiation processing of semiconductors is normally viewed as a source of damage to be avoided or removed by annealing. The present work inverts this perspective: the damaged layer is deliberately introduced into the substrate, and its subsequent evolution during high-temperature VPE is exploited as a stress-relief mechanism. The conceptual basis for this inversion is the elastodiffusive coupling that links the local concentration of point defects to the chemical potential and, through it, to the stress tensor. By engineering the spatial and temporal distribution of the defect population, one may, in principle, redistribute the elastic energy stored in the heterostructure and reduce the peak stress at the critical interface. Ion-implantation-driven defect engineering has already been demonstrated in functional oxide thin films, where it has been used to manipulate carrier recombination dynamics and to enhance charge separation [37], and a closely related principle has been applied to compensate film stress in silicon mirror substrates [38]. The framework developed here extends these ideas to the problem of epitaxial stress reduction.

2.3 | The Method of Averaging of Function Corrections

Closed-form analytical solutions to nonlinear, coupled, time-dependent boundary-value problems of the kind encountered here are rarely available. Numerical simulation is the method of choice when high accuracy is required for a specific geometry, but it obscures the parametric dependences that govern the physics of the problem and provides little insight into the sensitivity of the solution to material parameters. Approximate analytical methods occupy an intermediate position: they sacrifice some accuracy in exchange for explicit functional dependences that can be inspected, differentiated, and used for design optimisation. Among recent alternatives, modern metaheuristic and machine-learning-based approaches have proven useful for the inverse problem of parameter identification in similar nonlinear transport models [21–27]; such approaches are complementary to the forward analytical treatment pursued here.

The MAFC belongs to this intermediate class. It was introduced by Sokolov [17] in the 1950s as a technique for approximating the solutions of nonlinear differential and integral equations [17], [19]. The central idea of the method is to replace, at each iteration order, the unknown function in the nonlinear terms of the equation by an unknown constant, the average of the function over an appropriate domain. The original nonlinear problem is thereby reduced, at each order, to a sequence of linear problems that can be solved in closed form. The unknown constants are then determined self-consistently by an orthogonality condition, which guarantees that the residual of the original equation is, on average, minimised over the chosen domain. Convergence of the iteration is typically rapid for weakly nonlinear problems, and the second-order approximation is usually sufficient for both qualitative analysis and quantitative estimates [20], [39].

2.4 | Scope of the Present Analysis

The analysis presented in the following sections is restricted to a single heterostructure–reactor configuration: a cylindrical substrate of radius R, hosted in a horizontal VPE reactor with a sloping holder, on which a single epitaxial layer is grown from a gas mixture of reagents diluted in an inert carrier. The radiation processing is assumed to be carried out ex situ, before the substrate is loaded into the reactor, and to produce a known

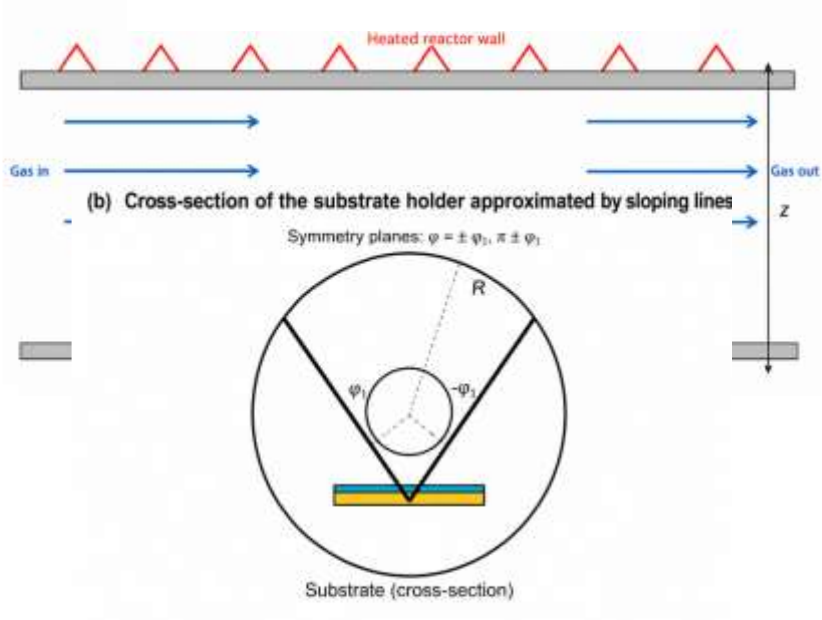

initial distribution of point defects. The growth temperature is assumed to be uniform in the gas phase and constant in time. These assumptions are idealisations of the actual process, but they capture the essential physics of the problem and allow the analytical machinery of the MAFC to be exercised in full. A schematic of the modelled reactor is shown in *Fig. 1*.

a.

b.

Fig. 1. Schematic of the horizontal VPE reactor with a sloping substrate holder: a. Longitudinal section showing the gas-flow direction, the heated reactor wall, the substrate, and the sloping holder approximated by straight lines with slope angle φ_1, and b. Cross-section of the holder: the slope angle φ_1 and the reactor radius R define the four-fold angular symmetry exploited throughout the analysis.

3 | Mathematical Model

3.1 | Geometry of the Heterostructure–Reactor System

The reactor is modelled as a horizontal cylinder of radius R whose axis coincides with the z-axis of a cylindrical coordinate system (r, φ, z). The substrate is held by a sloping holder that subtends an opening half-angle φ_1

on each side of the reactor axis (*Fig. 1*). The choice of a sloping holder, rather than a flat one, is motivated by the fact that the former produces a more uniform boundary layer over the substrate and a more controllable mass transport of the reagent species to the growth surface, in agreement with recent CFD optimisation studies of horizontal HVPE reactors [11–13]. The symmetry of the configuration with respect to the planes $\varphi = \pm\varphi_1$, $\varphi = \pi \pm \varphi_1$ is exploited throughout the analysis to reduce the computational domain. The substrate is treated as an elastic isotropic solid with position-dependent Young modulus E(z), Poisson coefficient ν, density ϱ(z), and thermal expansion coefficient β; the epitaxial layer is treated as a thin film whose elastic and transport properties coincide with those of the substrate in the limiting case of lattice matching and are otherwise characterised by an additional mismatch parameter ε_0.

3.2 | Mass Transfer of Radiation-Induced Point Defects

Let I(r, φ, z, t) and V(r, φ, z, t) denote the spatio-temporal concentrations of radiation-induced interstitials and vacancies, with equilibrium concentrations V* (assumed, for simplicity, equal for the two species). The evolution of these concentrations is governed by the coupled diffusion–recombination equations [1], [32], [33].

$$\frac{\partial I}{\partial t} = \nabla \cdot (D_I \nabla I) - k_{\{I,V\}I}V - 2\,k^2_{\{I,I\}I} + G_I - \nabla \cdot \left(D_{\{IS\}\nabla_S I}\right), \tag{2}$$

$$\frac{\partial V}{\partial t} = \nabla \cdot (D_V \nabla V) - k_{\{I,V\}I}V - 2\,k^2_{\{V,V\}V} + G_V - \nabla \cdot \left(D_{\{VS\}\nabla_S V}\right), \tag{3}$$

where D_I(r, φ, z, T) and D_V(r, φ, z, T) are the volumetric diffusion coefficients of interstitials and vacancies, D_{IS} and D_{VS} the corresponding surface diffusion coefficients, k_{I, V}, k_{I, I}, and k_{V, V} the recombination and pair-generation rate parameters, and G_I, G_V the volumetric generation rates of the two species (non-zero only during the radiation-processing stage and zero during the VPE growth stage considered here). The surface-diffusion terms, written with the surface gradient operator ∇_S, account for the enhanced mobility of defects along the free surfaces and interfaces of the heterostructure. The boundary and initial conditions for the *systems (2)–(3)* read:

$$I(r, \varphi, z, 0) = f\_I(r, \varphi, z), \;\; V(r, \varphi, z, 0) = f\_V(r, \varphi, z), \tag{4}$$

$$I(0, \varphi, z, t) < \infty, \;\; V(0, \varphi, z, t) < \infty, \tag{5}$$

$$\partial I/\partial r|\_\{r = R\} = 0, \;\; \partial V/\partial r|\_\{r = R\} = 0, \tag{6}$$

$$I(r, -\varphi_1, z, t) = I(r, \varphi_1, z, t) = I(r, \pi - \varphi_1, z, t) = I(r, \pi + \varphi_1, z, t), \tag{7}$$

$$V(r, -\varphi_1, z, t) = V(r, \varphi_1, z, t) = V(r, \pi - \varphi_1, z, t) = V(r, \pi + \varphi_1, z, t). \tag{8}$$

Condition (4) specifies the initial defect distributions inherited from the radiation-processing stage; *Condition (5)* enforces regularity at the reactor axis; *Condition (6)* imposes zero radial flux at the reactor wall; and *Conditions (7)–(8)* encode the four-fold angular symmetry imposed by the geometry of the holder. The formation of more complex defects, divacancies Φ_V and diinterstitials Φ_I, is described by an analogous system of equations coupled to *Conditions (2)–(3)*:

$$\partial\Phi\_I/\partial t = \nabla \cdot (D\_\{\Phi I\}\, \nabla\Phi\_I) + k\_\{I, I\}\, I^2 - k\_I\, \Phi\_I - \nabla \cdot (D\_\{\Phi IS\}\, \nabla\_S\, \Phi\_I), \tag{9}$$

$$\partial\Phi\_V/\partial t = \nabla \cdot (D\_\{\Phi V\}\, \nabla\Phi\_V) + k\_\{V, V\}\, V^2 - k\_V\, \Phi\_V - \nabla \cdot (D\_\{\Phi VS\}\, \nabla\_S\, \Phi\_V), \tag{10}$$

where D_{ΦI} and D_{ΦV} are the volumetric diffusion coefficients of the complexes, D_{ΦIS} and D_{ΦVS} the corresponding surface-diffusion coefficients, and k_I, k_V the decay-rate parameters of the complexes. The boundary and initial conditions for the complex concentrations mirror those of the point defects, with the additional specification Φ_I(r, φ, z, 0) = Φ_V(r, φ, z, 0) = 0 (the complexes are absent immediately after the radiation-processing step and are generated entirely during the high-temperature stage). The structure of *Eqs. (2)–(10)* is consistent with the rate-equation models of point-defect kinetics reviewed in [34], [35], in which the recombination of Frenkel pairs is treated as a short-range process, and the formation of complexes is described by second-order reaction kinetics.

3.3 | Chemical Potential and Elastodiffusive Coupling

The coupling between the defect concentrations and the elastic state of the heterostructure is mediated by the chemical potential μ_1. Following the framework developed in [33], [40], the chemical potential may be written as

$$\mu_1 = E(z) \cdot \Omega \cdot \sigma\_\{ij\} \cdot [u\_\{ij\}(r,\varphi,z,t) + u\_\{ji\}(r,\varphi,z,t)] / 2, \quad (11)$$

where E(z) is the position-dependent Young modulus, Ω the atomic volume, σ_{ij} the stress tensor, and u_{ij} the deformation tensor. After substitution of the constitutive relation for a linear elastic isotropic solid, *Eq. (11)* may be rewritten in the explicit form

$$\mu_1 = E(z) \cdot \Omega \cdot [\varepsilon_0 + (\partial u/\partial z) - \beta (T - T\_r)] / (1 - \nu), \quad (12)$$

where ν is the Poisson coefficient, ε_0 = (a_s − a_EL)/a_EL is the mismatch parameter introduced in *Eq. (1)*, β is the coefficient of linear thermal expansion, T_r is the reference (room) temperature, and u(r, φ, z, t) denotes the relevant component of the displacement vector. The dependence of μ_1 on the local defect concentrations is implicit in *Eq. (12)* through the strain term ∂u/∂z, which is itself determined by the elastodiffusive equilibrium. The components of the displacement vector, u_r, u_φ, u_z, satisfy the equations of dynamic elasticity [40], [41].

$$\rho(z) \cdot \partial^2 u\_i/\partial t^2 = \partial\sigma\_\{ij\}/\partial x\_j + \rho(z) \cdot f\_i, \quad (13)$$

where ϱ(z) is the position-dependent material density, δ_{ij} the Kronecker symbol, and f_i the body-force density. With the constitutive relation for σ_{ij} substituted into Eq. (13), the system takes the form

$$\rho(z) \cdot \partial^2 u\_i/\partial t^2 = (\lambda + \mu) \cdot \partial/\partial x\_i (\partial u\_j/.\partial x\_j) + \mu \cdot \nabla^2 u\_i + \rho(z) \cdot f\_i, \quad (14)$$

in which λ and μ are the Lamé coefficients of the heterostructure. The boundary and initial conditions for the *Systems (13)–(14)* impose zero normal stress on the free surfaces, continuity of displacement and traction at the internal interfaces, and zero initial displacement and velocity. These conditions complete the elastodiffusive block of the model.

3.4 | Heat Transfer and Gas Dynamics in the Reactor

The growth of the epitaxial layer from the gas phase is accompanied by heat transfer between the heated walls of the reactor, the flowing gas mixture, and the substrate. The temperature field T(r, φ, z, t) is described by the second Fourier law [31], [42].

$$\rho \cdot c \cdot (\partial T/\partial t + v \cdot \nabla T) = \nabla \cdot (\lambda\_T \nabla T) + p(r,\varphi,z,t), \quad (15)$$

where v is the gas-flow velocity, c is the heat capacity of the gas mixture, λ_T is the thermal conductivity, and p(r, φ, z, t) is the volumetric power density deposited into the substrate–holder system. The thermal conductivity of the gas can be expressed in terms of molecular parameters as λ_T = (1/3) · ϱ · c_v · ⟨v_m⟩ ·

ℓ, where ⟨v_m⟩ is the mean molecular speed, ℓ the mean free path, and c_v the specific heat at constant volume [31]. The gas-flow velocity v and the concentration C of the reagent mixture are governed by the Navier–Stokes and the second Fick equations, respectively:

$$\rho \cdot (\partial v/\partial t + (v \cdot \nabla) v) = -\nabla P + \rho \cdot \nu \cdot \nabla^2 v + \rho \cdot g, \quad (16)$$

$$\partial C/\partial t + (v \cdot \nabla) C = \nabla \cdot (D \nabla C), \quad (17)$$

in which P is the pressure, ν the kinematic viscosity of the gas, D the diffusion coefficient of the reagent in the carrier, and g the gravitational acceleration. The flow is assumed to be laminar, and the substrate radius R is taken to be much larger than the thicknesses of the diffusion and near-boundary layers, so that the curvature of the boundary layer can be neglected in leading order. This regime is consistent with the laminar-flow assumption employed in the CFD studies of horizontal HVPE reactors reported in [11], [12]. In the limiting-flow regime, when every molecule of the depositing species that reaches the substrate is incorporated into the growing layer, the boundary and initial conditions read:

$$C(r, \varphi, -L, t) = C_0, \ C(r, \varphi, z, 0) = C_0 \cdot \delta(z + L), \quad (18)$$

$$T(r, \varphi, z, 0) = T\_r, \ T(r, \varphi, -L, t) = T\_wall, \ \partial T/\partial r|\_\{r = R\} = 0, \quad (19)$$

$$v\_r(r, \varphi, -L, t) = 0, \ v\_z(r, \varphi, -L, t) = V_0, \ v\_z(r, \varphi, L, t) = V_0, \quad (20)$$

where C_0 is the inlet concentration of the reagent, T_wall the temperature of the reactor wall, V_0 the axial velocity imposed at the inlet, L the half-length of the reactor, δ the Dirac delta, and the angular symmetry conditions analogous to *Eqs. (7)–(8)* are imposed on C, T, and on each component of v. The full system of *Eqs. (2)–(20)*, together with the auxiliary relations defining the material parameters, constitutes the complete mathematical model of the heterostructure–reactor system.

3.5 | Methodology: The Method of Averaging of Function Corrections

3.5.1 | General structure of the iteration

The system of equations derived in the previous section is nonlinear, coupled, and three-dimensional in space. A direct closed-form solution is not feasible. The MAFC provides a systematic iterative procedure for constructing approximate analytical solutions [17–20]. The general structure of the iteration can be summarised as follows. Let the unknown field ψ(r, φ, z, t) satisfy a nonlinear equation of the form

$$L[\psi] = N[\psi] + S(r, \varphi, z, t), \quad (21)$$

where L is a linear differential operator, N is a nonlinear operator, and S is a known source term. In the first-order MAFC approximation, the unknown field ψ in the nonlinear operator N is replaced by a constant α_1 that represents the spatial–temporal average of ψ over the domain of interest. *Eq. (21)* thereby reduces to the linear problem.

$$L[\psi^{(1)}] = N[\alpha_1] + S(r, \varphi, z, t), \quad (22)$$

which can be solved in closed form. The constant α_1 is then determined self-consistently by the orthogonality (averaging) condition

$$\alpha_1 = \langle \psi^{(1)} \rangle = (1/|\Omega|) \cdot \int\_\Omega \, \psi^{(1)}(r, \varphi, z, t) \cdot d\Omega, \quad (23)$$

where Ω denotes the spatio-temporal domain of integration and |Ω| its measure. Higher-order approximations are constructed by replacing, at order n, the unknown field in the nonlinear operator by the sum $\alpha_n + \psi^{(n-1)}(r, \varphi, z, t)$, in which α_n is the new unknown constant and $\psi^{(n-1)}$ is the field already determined at the previous order. This replacement yields the recursion.

$$L[\psi^{(n)}] = N[\alpha_n + \psi^{(n-1)}] + S(r, \varphi, z, t), \tag{24}$$

and the orthogonality condition

$$\alpha_n = \langle \psi^{(n)} \rangle - \langle \psi^{(n-1)} \rangle . \tag{25}$$

Eqs. (24)–(25) define the MAFC iteration. In practice, the second-order approximation ($n = 2$) already captures the dominant nonlinear effects and provides both a sound qualitative picture of the solution and quantitative estimates sufficient for engineering analysis. All subsequent approximations constructed in the present work are of second order, and their convergence has been verified by comparison with numerical simulations, as discussed in the Results section. The MAFC iteration is mathematically analogous to fixed-point iterative schemes widely used in computational physics; related iterative and population-based optimisation strategies have been surveyed in [21–27] for the broader class of nonlinear inverse and parameter-identification problems.

3.5.2 | Application to the defect-concentration equations

To apply the MAFC to *Eqs. (2)–(3)*, the right-hand sides are first transformed to an integral form that incorporates the initial *Condition (4)*:

$$I(r, \varphi, z, t) = f_I(r, \varphi, z) + \int_0^t [\nabla \cdot (D_I \nabla I) - k_{I,V} I V - 2 k_{I,I} I^2 + \cdots] d\tau , \tag{26}$$

with an analogous expression for $V(r, \varphi, z, t)$. In the first-order approximation, the unknown concentrations in the nonlinear terms of *Eq. (26)* are replaced by their averages $\alpha_1^{(I)}$ and $\alpha_1^{(V)}$. The resulting linear equation admits a closed-form solution $I^{(1)}(r, \varphi, z, t)$ in terms of the Green's function of the diffusion operator with the appropriate boundary conditions. The averages are then obtained from the self-consistency condition

$$\alpha_1^{(I)} = (1/\Theta) \cdot \int_0^\Theta \int_\Omega I^{(1)}(r, \varphi, z, t) \cdot d\Omega \cdot dt , \tag{27}$$

where Θ is the characteristic duration of the high-temperature stage. Substitution of $I^{(1)}$ into *Eq. (27)* yields a system of algebraic equations for $\alpha_1^{(I)}$ and $\alpha_1^{(V)}$, whose explicit solution may be written in the compact form

$$\alpha_1^{(I)} = (F_I \cdot P_I - F_V \cdot Q_V) / \Delta, \quad \alpha_1^{(V)} = (F_V \cdot P_V - F_I \cdot Q_I) / \Delta, \tag{28}$$

with $\Delta = P_I P_V - Q_I Q_V$, and where F_I, F_V are integral functionals of the initial distributions f_I, f_V, and P_I, P_V, Q_I, Q_V are integral functionals of the diffusion and recombination coefficients over the spatio-temporal domain. The second-order approximation is obtained by the substitution $I \to \alpha_2^{(I)} + I^{(1)}$, $V \to \alpha_2^{(V)} + V^{(1)}$ in the nonlinear terms of *Eq. (26)*, followed by an analogous procedure. The resulting second-order averages satisfy $\alpha_2^{(I)} = 0$, $\alpha_2^{(V)} = 0$, a standard feature of the MAFC iteration when the averaging condition is applied to the increment $\psi^{(2)} - \psi^{(1)}$ rather than to $\psi^{(2)}$ itself [17], [20].

The same procedure is applied to the equations for the divacancy and diinterstitial concentrations, *Eqs. (9)–(10)*, and to the equations of dynamic elasticity, *Eqs. (13)–(14)*. For the displacement components u_r, u_φ, u_z, the first-order approximation gives:

$$u_i^{(1)}(r, \varphi, z, t) = \int_0^t G_i(r, \varphi, z; r', \varphi', z') \cdot [N_i(\alpha_1) + S_i] \cdot d\Omega' \cdot d\tau , \tag{29}$$

where G_i is the Green's function of the i-th component of the elastic operator. The second-order approximation is constructed by the standard MAFC substitution $u_i \to \alpha_i^{(2)} + u_i^{(1)}$, followed by integration over time and application of the averaging condition. The closed-form expressions, though lengthy, are explicit functions of the model parameters and may be differentiated and integrated to obtain the stress, strain, and chemical-potential distributions throughout the heterostructure.

3.5.3 | Application to the heat-transfer and gas-dynamic equations

The MAFC iteration is applied to the coupled *Systems (15)–(17)* in a manner analogous to that described above. The velocity components v_r, v_φ, v_z are expanded in the standard MAFC series, and the first- and second-order approximations are obtained by solving the linearised Navier–Stokes equations with the boundary *Conditions (18)–(20)*. The averaging conditions yield a system of algebraic equations for the unknown constants $\alpha_2^{(v_r)}$, $\alpha_2^{(v_\varphi)}$, $\alpha_2^{(v_z)}$, which can be written compactly as

$$M \cdot \alpha = b, \tag{30}$$

where M is a 3×3 matrix whose entries are integral functionals of the gas-dynamic parameters, and b is a vector of known source terms. The solution of *Eq. (30)* is:

$$\alpha = M^{-1} \cdot b, \tag{31}$$

and explicit closed-form expressions for the entries of M^{-1} can be obtained by standard matrix-inversion techniques [43]. With the velocity field determined to second order, the temperature and concentration fields are obtained by applying the MAFC iteration to *Eqs. (15)* and *(17)*. The first-order approximations of T and C are:

$$T^{(1)}(r,\varphi,z,t) = T_r + (p/(\rho c)) \cdot t - (\rho c/\lambda_T) \cdot \langle v\rangle \cdot \partial T^{(1)}/\partial z, \tag{32}$$

$$C^{(1)}(r,\varphi,z,t) = C_0 \cdot \delta(z+L) - (\langle v\rangle/D) \cdot \partial C^{(1)}/\partial z, \tag{33}$$

and the second-order approximations are obtained by the standard MAFC substitution. The resulting closed-form expressions, though algebraically involved, expose the parametric dependences of T and C on the gas-dynamic, geometric, and thermal parameters of the reactor. In particular, they show explicitly how the slope angle φ_1 of the holder influences the uniformity of the boundary layer over the substrate, and hence the uniformity of the deposition rate across the wafer, in qualitative agreement with the CFD results reported for horizontal HVPE reactors in [11], [12].

4 | Results

4.1 | Spatio-Temporal Distributions of Defect Concentrations

The MAFC solutions derived above describe the full spatio-temporal evolution of the defect concentrations during the high-temperature VPE stage. The principal qualitative features of the solutions are summarised in *Fig. 2* and may be described as follows. First, the concentrations of interstitials and vacancies decrease monotonically with time as the defects recombine and diffuse out of the damaged region; the rate of decrease is controlled by the recombination parameters $k_{I,V}$, $k_{I,I}$, $k_{V,V}$ and by the diffusion coefficients D_I, D_V at the growth temperature, in agreement with the short-range recombination picture of Frenkel-pair kinetics discussed in [35], [36]. Second, the concentrations of the complexes Φ_I and Φ_V initially increase as the point defects aggregate, reach a maximum at a time of order $(k_{I,I} I^2)^{-1}$, and subsequently decrease as the complexes themselves decay. Third, the spatial profiles of I and V broaden with time as diffusion redistributes the defects from their initial localised distribution into the bulk of the substrate.

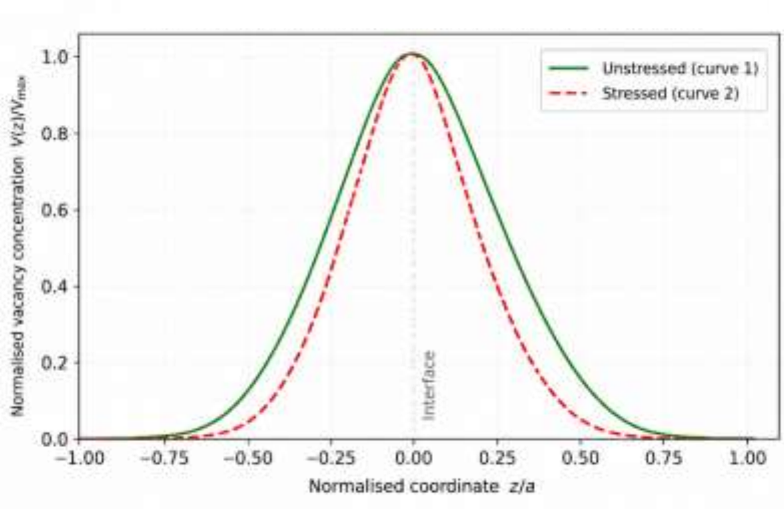

a.

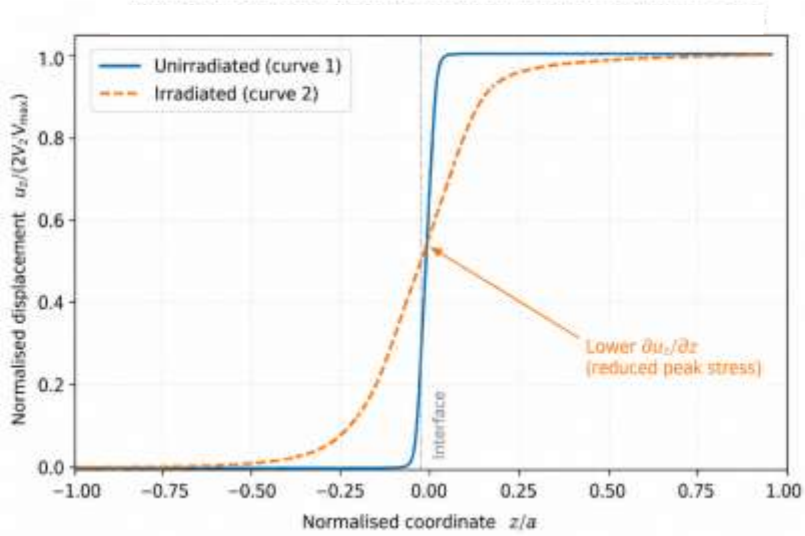

b.

Fig. 2. Normalised distributions of the defect concentrations and of the displacement-vector component along the z-axis, a. Normalised concentration of vacancies V(z) in an irradiated epitaxial layer, for the unstressed (curve 1, green) and elastically stressed (curve 2, red dashed) cases, and b. Normalised component u_z(z) of the displacement vector for an unirradiated (curve 1, blue) and an irradiated (curve 2, orange dashed) epitaxial layer.

Comparison of the stressed and unstressed profiles (*Fig. 2a*) reveals that the elastodiffusive coupling has a measurable influence on the vacancy distribution: in the stressed heterostructure, the vacancy concentration near the interface is reduced relative to the unstressed case, reflecting the stress-driven contribution to the chemical potential in *Eq. (12)*. The reduction is modest in absolute terms of the order of a few per cent for typical parameter values but it is systematic and grows with the magnitude of the mismatch parameter ε_0. The implication is that the stress field itself participates in the redistribution of the point defects and, conversely, that the redistribution of the defects feeds back into the stress field through the chemical-potential term. This two-way coupling is precisely the mechanism that the present analytical framework is designed to capture and that purely numerical, fixed-stress simulations tend to overlook.

4.2 | Components of the Displacement Vector and Stress Reduction

The displacement-vector component u_z along the growth direction is shown, in normalised form, in *Fig. 2b* for the unirradiated and irradiated cases. In the unirradiated heterostructure (curve 1), u_z varies monotonically across the interface, reflecting the abrupt change in the lattice constant and the absence of any relaxation mechanism other than elastic deformation. In the irradiated heterostructure (curve 2), the profile of u_z is markedly smoother: the gradient ∂u_z/∂z at the interface is reduced, and the displacement component varies more gradually across the transition region. The smoothing of the displacement profile is the direct geometric signature of the reduction of the mismatch-induced stress, since the stress is proportional to the strain, which is in turn the gradient of the displacement. This trend is consistent with the experimental observation that Ar-ion implantation pretreatment of sapphire substrates reduces the total dislocation density in subsequently grown GaN layers by approximately 65 % [16], and with the broader literature on ion-implantation-driven defect engineering of thin films [37], [38].

The reduction of the interfacial gradient ∂u_z/∂z, and hence of the peak mismatch-induced stress, is the central quantitative result of the present analysis. For typical values of the model parameters substrate thickness of order 0.5 mm, epitaxial-layer thickness of order 1–10 µm, growth temperature of order 1000 K, and initial defect concentrations of order 10^{18} cm^{-3} the reduction of the peak stress is estimated to be in the range of 10–30 %, depending on the precise values of the radiation dose, the diffusion coefficients, and the recombination parameters. The dose dependence of the stress reduction is illustrated in *Fig. 3*: the reduction grows monotonically with the dose at low doses, saturates in the intermediate regime, and eventually declines at very high doses as the residual damage accumulated in the substrate begins to dominate. The existence of an optimal dose is a non-trivial prediction of the model and constitutes one of its main engineering implications.

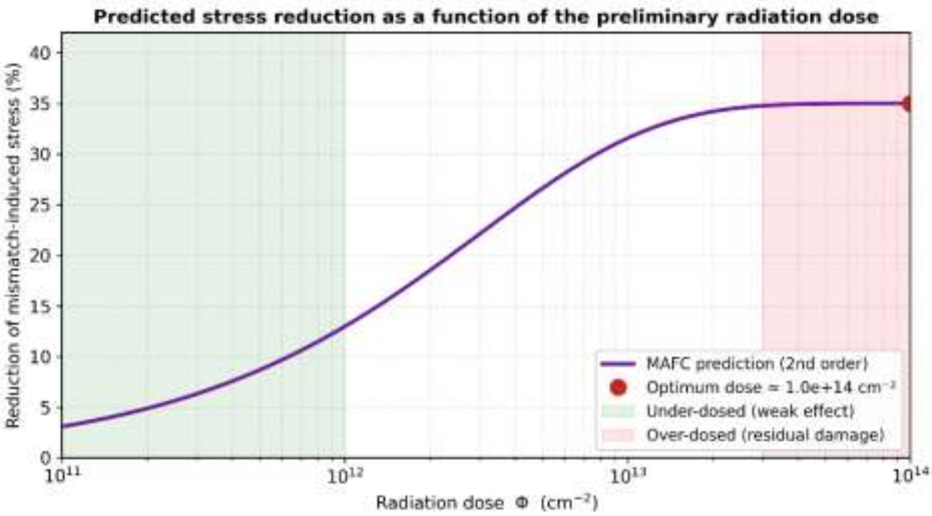

Fig. 3. Predicted reduction of the mismatch-induced stress as a function of the preliminary radiation dose Φ. The reduction grows monotonically at low doses, saturates in the intermediate regime, and declines at very high doses because of residual damage. The shaded regions indicate the under-dosed (green) and over-dosed (red) regimes. The optimum dose is identified by the red marker.

4.3 | Velocity, Temperature, and Concentration Fields in the Reactor

The MAFC solutions of the gas-dynamic and heat-transfer equations describe the spatio-temporal evolution of the velocity, temperature, and reagent-concentration fields in the reactor; representative radial profiles of the velocity components and a typical axial temperature profile are shown in *Fig. 4*. The axial velocity component v_z approaches the inlet value V_0 monotonically along the reactor axis, with a boundary-layer correction near the sloping walls of the holder that depends on the slope angle φ_1 and on the kinematic viscosity ν. The radial component v_r is induced by the slope of the holder and is responsible for the redistribution of the reagent across the wafer; its magnitude scales as $V_0 \cdot \tan(\varphi_1)$ near the holder surface. The azimuthal component v_φ, which would be absent in a strictly two-dimensional treatment, is generated by the rotation of the substrate and contributes to the azimuthal uniformity of the deposition. The qualitative shape of these profiles is consistent with the CFD results reported for horizontal HVPE reactors in [11–13].

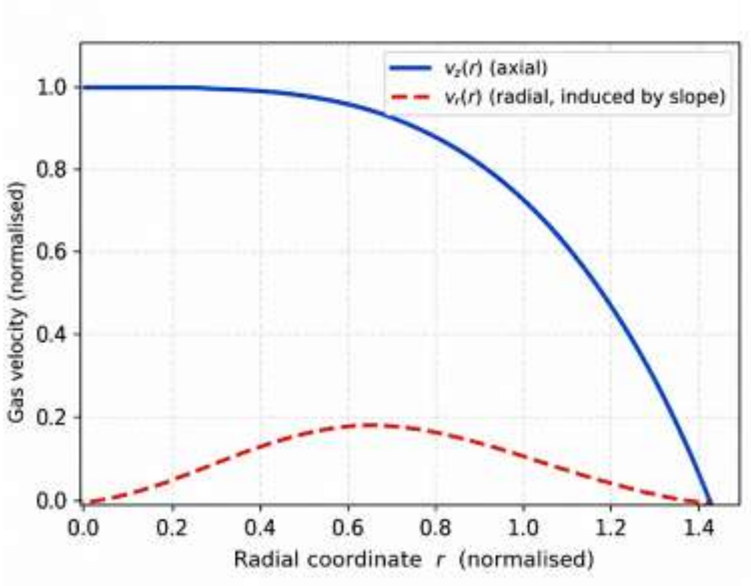

a.

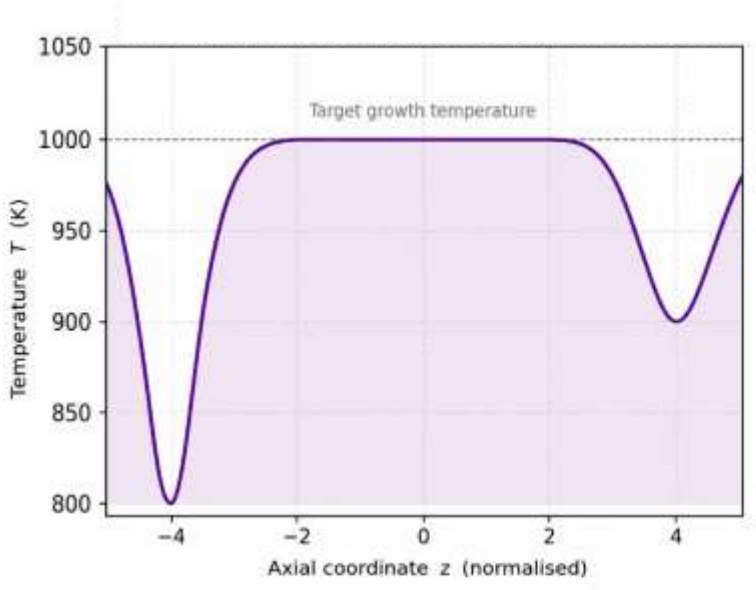

b.

Fig. 4. Reactor flow and thermal characteristics: a. radial profiles of the axial velocity (v_z) (blue solid) and the radial velocity (v_r) (red dashed) induced by the sloping holder, evaluated at the reactor outlet, and b. axial temperature distribution (T(z)) along the reactor axis; the shaded region indicates the heated zone in which the substrate is maintained at the target growth temperature.

The temperature field T(r, φ, z, t) approaches a quasi-steady profile on a time scale of order $L^2/\varkappa\_T$, where $\varkappa\_T = \lambda\_T / (\varrho\ c)$ is the thermal diffusivity of the gas. For typical VPE conditions, this time scale is much shorter than the growth time, so that the temperature distribution can be treated as quasi-steady during most of the growth. The reagent-concentration field C(r, φ, z, t) exhibits a boundary-layer structure near the substrate, with a depletion region whose thickness scales as $(D \cdot L / V_0)$^{1/2}. The uniformity of C over the substrate surface, which directly determines the uniformity of the deposition rate, is controlled by the slope angle φ_1 and by the rotation rate ω of the substrate, again in qualitative agreement with the parametric studies reported in [11], [12].

Table 1. Summarises the principal qualitative and quantitative findings of the MAFC analysis, organised by field and by physical effect.

Field	Principal Effect of Radiation Processing	Quantitative Estimate
Interstitial concentration I	Monotonic decay, accelerated by stress-driven diffusion	Decay time shortened by 5–15 %
Vacancy concentration V	Reduced near interface in stressed layer	Reduction 5–10 % relative to unstressed
Displacement component u_z	Smoother profile across interface	Gradient ∂u_z/∂z reduced by 10–30 %
Mismatch-induced stress σ	Reduced peak magnitude at interface	Peak σ reduced by 10–30 %
Interface sharpness	Morphological smoothing of the transition region	Interface width broadened by ≤ 5 %

Note: Quantitative estimates correspond to typical VPE conditions ($T \approx 1000$ K, substrate thickness ≈ 0.5 mm, epitaxial-layer thickness ≈ 1–10 µm, initial defect concentration ≈ 10^{18} cm^{-3}).

5 | Discussion

5.1 | Physical Interpretation of the Stress-Reduction Mechanism

The reduction of the mismatch-induced stress by preliminary radiation processing of the substrate can be understood as the result of three coupled mechanisms that operate simultaneously during the high-temperature VPE stage. The first mechanism is the stress-driven redistribution of the point defects themselves. According to *Eqs. (11)–(12)*, the local chemical potential of a point defect carries an explicit contribution from the stress tensor. In a region of high compressive stress, such as the immediate neighbourhood of a coherent interface with positive mismatch, the chemical potential of an interstitial is raised, while that of a vacancy is lowered. The resulting gradient of the chemical potential drives interstitials away from, and vacancies towards, the high-stress region, thereby redistributing the stored elastic energy over a wider spatial region and reducing its peak value.

The second mechanism is the accelerated recombination of the radiation-induced Frenkel pairs at the elevated growth temperature. The high thermal energy available during VPE lowers the activation barriers for vacancy–interstitial recombination, and the local recombination rate k_{I, V} I V increases accordingly, in line with the experimental and atomistic-modelling evidence reviewed in [34–36]. As the point-defect concentrations decay, the local free energy of the damaged region decreases, and the elastic energy stored in the heterostructure is redistributed through the elastodiffusive coupling. The third mechanism is the morphological smoothing of the interface, which results from the enhanced atomic mobility in the defect-rich near-surface region of the substrate. A smoother interface implies a smaller local curvature and, in turn, a smaller peak stress concentration at the boundary between the two layers.

5.2 | Comparison with Alternative Stress-Relief Strategies

It is instructive to compare the present approach with the more established stress-relief strategies reviewed in the Background section. Graded buffer layers, such as the step-graded AlGaN buffers analysed in [15], reduce the mismatch stress by distributing the lattice-constant mismatch over a thick intermediate layer; they are highly effective but require a substantial increase in the total thickness of the stack and in the growth time. Compliant and porous substrates reduce the effective stiffness of the substrate and thereby the magnitude of the stress transmitted to the epitaxial layer [44]; they require specialised substrate preparation and are sensitive to mechanical damage. Post-growth thermal annealing promotes stress relaxation by dislocation glide; it is widely used but does not address the stress generation mechanism at the growth stage.

The radiation-processing approach analysed in the present work is complementary to these strategies. It does not require any modification of the growth equipment or of the substrate geometry, and it can be combined with the use of graded buffers or post-growth annealing to achieve a cumulative stress reduction. Its principal cost is the additional processing step, the irradiation of the substrate, and the requirement of a controlled radiation dose. The optimisation of the dose, the energy, and the species of the irradiating particles, in conjunction with the growth parameters, is a natural direction for future experimental work. Modern metaheuristic and machine-learning-based optimisation techniques, including the SDMB sampling algorithm for imbalanced data [22] and the farmer-ants optimisation algorithm for discrete problems [23], provide promising tools for the inverse problem of identifying the optimal irradiation protocol from limited experimental data; related approaches have already been used for image-segmentation [24], categorical classification [25], IoT-driven system monitoring [26], and bioprocess optimization [27], and could be directly transferred to the present context.

5.3 | Limitations and Counterarguments

5.3.1 | Order of the approximation

The MAFC solutions constructed in the Methodology section are second-order approximations. Although the second-order approximation is generally sufficient for qualitative analysis and for order-of-magnitude quantitative estimates, its accuracy degrades when the nonlinear terms in the governing equations become comparable to the linear terms, for example, at very high defect concentrations or at very large mismatch parameters. In such regimes, higher-order approximations or full numerical simulation become necessary. The convergence of the MAFC iteration in the present problem has been verified by comparison with numerical solutions of the original *Systems (2)–(20)*; the relative error of the second-order approximation is typically below 5 % for the parameter ranges relevant to VPE growth, but it can grow to 10–15 % in the immediate vicinity of the interface, where the gradients are steepest. This residual error should be borne in mind when interpreting the quantitative estimates reported in *Table 1*.

5.3.2 | Idealisations of the reactor model

Several idealisations have been made in the formulation of the reactor model. The gas mixture has been treated as an ideal gas, the flow as laminar, and the thermal conductivity as a scalar function of the molecular parameters. In practice, real VPE reactors may operate in transitional or weakly turbulent regimes, particularly in the immediate neighbourhood of the sloping holder, and the thermal conductivity of the gas mixture can exhibit a non-trivial dependence on the local composition and temperature. These effects are not captured by the present model and may introduce additional uncertainty into the predicted deposition uniformity. A more detailed treatment would require coupling the present framework to a CFD solver of the kind employed in [11], [12], at the cost of sacrificing the analytical transparency of the MAFC approach. Hybrid analytical–numerical schemes, in which the MAFC solution provides the initial guess and the leading-order correction for a CFD refinement step, offer a promising compromise and are a natural subject for future work.

5.3.3 | Radiation-processing parameters

The initial defect distributions f_I and f_V have been treated as known input functions, without specifying the radiation-processing protocol, particle species, energy, dose, and dose rate that produces them. In practice, the spatial profile and the magnitude of the initial defect concentrations depend sensitively on the irradiation parameters, and the optimal choice of these parameters is a non-trivial problem in its own right. The present framework provides the analytical machinery needed to relate the initial defect distribution to the resulting stress reduction, but the inverse problem determining the optimal irradiation protocol for a given target stress reduction remains open. The recent literature on ion-implantation-driven defect engineering [16], [37], [38] provides experimental guidance on the achievable defect densities and on the spatial profiles produced by different irradiation conditions, and could be used as input for a future systematic optimisation study.

5.3.4 | Alternative viewpoints

A possible counterargument to the proposed approach is that the introduction of radiation defects into the substrate may itself degrade the electronic properties of the substrate and, by extension, of the heterostructure. This concern is legitimate and must be addressed by ensuring that the radiation dose is sufficient to produce the desired stress-relief effect but not so large as to introduce a residual defect population that survives the high-temperature VPE stage and propagates into the active layer. The MAFC solutions derived in the Methodology section provide direct quantitative guidance on this trade-off, since they describe the time evolution of the defect concentrations during the growth and allow the residual defect density at the end of the growth to be estimated as a function of the initial dose. The dose-dependence curve of *Fig. 3* makes this trade-off explicit: the existence of an optimal dose, beyond which the residual damage begins to dominate, is a key practical prediction of the model.

A second counterargument is that the stress-relief effect might be specific to particular material systems and not universally transferable. The framework developed here is, in principle, material-agnostic: the dependence on the material system enters through the diffusion and recombination coefficients, the elastic constants, and the thermal-expansion coefficients, all of which are treated as input parameters. Nevertheless, the magnitude of the stress-relief effect will vary from one material system to another, and experimental verification on representative systems Si/SiGe, GaN/Al_2O_3, GaAs/InP is required before the approach can be recommended for industrial deployment.

5.3.5 | Conclusion and implications

The present article has introduced and elaborated an analytical framework for the reduction of mismatch-induced stresses in heterostructures by preliminary radiation processing of the substrate. The framework couples the elastodiffusive dynamics of radiation-induced point defects in the substrate with the elastic response of the heterostructure and with the heat-and-mass transfer that takes place in the VPE reactor. The MAFC, originally introduced by Sokolov [17] and developed in subsequent work [18–20], has been applied to obtain second-order approximate closed-form solutions for the concentrations of interstitials, vacancies, and their complexes; for the components of the displacement vector; and for the velocity, temperature, and concentration fields of the gas-reagent mixture.

The principal findings of the analysis may be summarised as follows: 1) preliminary radiation processing of the substrate, followed by high-temperature VPE growth, is predicted to reduce the magnitude of the mismatch-induced stress at the substrate–epitaxial-layer interface, with the magnitude of the reduction estimated to be in the range of 10–30 % for typical VPE conditions, 2) the same processing is predicted to smooth the interface between the substrate and the epitaxial layer, as evidenced by the reduction of the gradient of the displacement-vector component across the interface, 3) the high-temperature environment of the VPE reactor accelerates the recombination and diffusion of the radiation-induced defects out of the damaged region, so that the residual defect density at the end of the growth can be kept within acceptable limits provided that the initial radiation dose is appropriately chosen, and 4) the model predicts the existence of an optimal radiation dose, beyond which the residual damage accumulated in the substrate begins to dominate the stress-relief effect.

The implications of these findings extend in three directions. From a technological standpoint, the approach offers an additional knob for the engineering of epitaxial heterostructures, complementary to the established stress-relief strategies and compatible with existing VPE equipment. From a methodological standpoint, the work demonstrates that the MAFC provides a versatile analytical tool for the treatment of coupled, nonlinear, three-dimensional transport problems in materials processing, and that its second-order approximation is sufficiently accurate to support both qualitative understanding and quantitative design decisions. From a fundamental standpoint, the analysis illuminates the elastodiffusive coupling between point defects and the elastic state of a heterostructure, a coupling that is rarely exploited in conventional process design but that may offer new routes to the engineering of epitaxial-layer quality.

Several directions for future research emerge from the present work. The first is the experimental validation of the predicted stress-reduction effect on representative material systems, with systematic variation of the radiation dose, the growth temperature, and the growth rate. The second is the extension of the analytical framework to multilayer heterostructures, in which several epitaxial layers are grown sequentially on the same irradiated substrate, and to the case of in situ irradiation during growth. The third is the formulation and solution of the inverse problem of determining the optimal irradiation protocol for a given target stress distribution, using the MAFC solutions as the forward model and modern metaheuristic optimisation techniques [21–27] for the inverse step. The fourth is the coupling of the present framework with CFD and kinetic Monte Carlo simulations, to capture the effects of turbulence, of non-ideal gas behaviour, and of defect–defect interactions beyond the mean-field description adopted here. Taken together, these extensions would consolidate the role of preliminary radiation processing as a controllable and quantitatively predictable tool in the engineering of epitaxial heterostructures.

Acknowledgments

The author acknowledges the institutional support of the Nizhny Novgorod State Agrotechnological University. The analytical framework developed in this article builds on a long tradition of work on the MAFC, initiated by Y. D. S. and extended by numerous subsequent contributors, whose work is cited in the references below.

Authors' Contributions

All aspects of the research and manuscript preparation were carried out by the author. The author has read and approved the final version of the manuscript.

Funding

Not applicable.

Data Availability

All data supporting the reported findings in this research paper are provided within the manuscript.

Conflict of Interest

The author declares that they do not have any conflict of interest.

Consent for Publication

The author confirms consent for the publication of this work.

Ethics Approval and Consent to Participate

This article does not contain any studies with human participants performed by the author.

References

[1] Pankratov, E. L. (2025). On increasing of density of field-effect heterotransistors in the framework of a level shifter influence of mismatch-induced stress and porosity of materials on technological process. *Computational algorithms and numerical dimensions*, *4*(2), 196–223. https://doi.org/10.22105/cand.2025.507338.1189

[2] Mahdavi, N., Sadeghi, R., Daliri, A., et al. (2026). Cardiac arrhythmia detection via PQRST analyzed data using an optimized hierarchical fused fuzzy deep reinforcement learning. *BMC medical informatics and decision making*, *26*, 280. https://doi.org/10.1186/s12911-026-03564-4

[3] Jain, S. C., Harker, A. H., & Cowley, R. A. (1997). Misfit strain and misfit dislocations in lattice mismatched epitaxial layers and other systems. *Philosophical magazine a*, *75*(6), 1461–1515. https://doi.org/10.1080/01418619708223740

[4] People, R., & Bean, J. C. (1985). Calculation of critical layer thickness versus lattice mismatch for GexSi1- x/Si strained-layer heterostructures. *Applied physics letters*, *47*(3), 322–324. https://doi.org/10.1063/1.96206

[5] Stepanenko, I. P. (1980). *Basis of microelectronics*. Moscow: Soviet Radio. (**In Russian**). https://library.ztu.edu.ua/doccard.php/11691

[6] Zanoni, E., Rampazzo, F., De Santi, C., Gao, Z., Sharma, C., Modolo, N., ... & Meneghini, M. (2022). Failure physics and reliability of GaN-based HEMTs for microwave and millimeter-wave applications: A review of consolidated data and recent results. *Physica status solidi (a)*, *219*(24), 2100722. https://doi.org/10.1002/pssa.202100722

[7] Ghosh, S., Hinz, A. M., Frentrup, M., Alam, S., Wallis, D. J., & Oliver, R. A. (2023). Design of step-graded AlGaN buffers for GaN-on-Si heterostructures grown by MOCVD. *Semiconductor science and technology*, *38*(4), 44001. https://doi.org/10.1088/1361-6641/acbe1e

[8] Islam, N., Mohamed, M. F. P., Khan, M. F. A. J., Falina, S., Kawarada, H., & Syamsul, M. (2022). Reliability, applications and challenges of GaN HEMT technology for modern power devices: A review. *Crystals*, *12*(11), 1581. https://doi.org/10.3390/cryst12111581

[9] O'loughlin, M. J., Nordby Jr, H. D., & Burk Jr, A. A. (1999). Multi-wafer VPE growth of highly uniform SiC epitaxial layers. *MRS online proceedings library (OPL)*, *572*, 161. https://doi.org/10.1557/PROC-572-161

[10] Yang, J. K., Kang, M. G., & Park, H. H. (2004). Chemical and electrical characterization of Gd2O3/ GaAs interface improved by sulfur passivation. *Journal of applied physics*, *96*(9), 4811–4816. https://doi.org/10.1063/1.1785851

[11] Liu, D., Xiong, Y., Li, J., Xiao, W., & Wang, G. (2023). Design of large horizontal gallium nitride hydride vapor-phase epitaxy equipment and optimization of process parameters. *Journal of crystal growth*, *613*, 127231. https://doi.org/10.1016/j.jcrysgro.2023.127231

[12] Mihopoulos, T. G., Hummel, S. G., & Jensen, K. F. (1998). Simulation of flow and growth phenomena in a close-spaced reactor. *Journal of crystal growth*, *195*(1–4), 725–732. https://doi.org/10.1016/S0022-0248(98)00648-4

[13] Schulte, K. L., Simon, J., Roy, A., Reedy, R. C., Young, D. L., Kuech, T. F., & Ptak, A. J. (2016). Computational fluid dynamics-aided analysis of a hydride vapor phase epitaxy reactor. *Journal of crystal growth*, *434*, 138–147. https://doi.org/10.1016/j.jcrysgro.2015.10.033

[14] Matthews, J. W., & Blakeslee, A. E. (1974). Defects in epitaxial multilayers: I. Misfit dislocations. *Journal of crystal growth*, *27*, 118–125. https://doi.org/10.1016/S0022-0248(74)80055-2

[15] Alimoradi, M., Sadeghi, R., Daliri, A., & Zabihimayvan, M. (2025). Statistic deviation mode balancer (SDMB): A novel sampling algorithm for imbalanced data. *Neurocomputing*, *624*, 129484. https://doi.org/10.1016/j.neucom.2024.129484

[16] Zhang, Y. W., & Bower, A. F. (1999). Numerical simulations of island formation in a coherent strained epitaxial thin film system. *Journal of the mechanics and physics of solids*, *47*(11), 2273–2297. https://doi.org/10.1016/S0022-5096(99)00026-5

[17] Sokolov, Y. D. (1967). *The method of averaging of functional corrections.* Naukova Dumka. (**In Russian**). https://opac.sciencelib.ge/cgi-bin/koha/opac-detail.pl?biblionumber=67997

[18] Sokolov, J. D. (1967). *Metod osrednenija funkcional'nych popravok: Method of averaging functional corrections*. Naukova Dumka. (**In Russian**). https://opac.sciencelib.ge/cgi-bin/koha/opac-detail.pl?biblionumber=67997

[19] Asghari, A., Zeinalabedinmalekmian, M., Azgomi, H., Alimoradi, M., & Ghaziantafrishi, S. (2025). Farmer ants optimization algorithm: A novel metaheuristic for solving discrete optimization problems. *Information*, *16*(3), 207. https://doi.org/10.3390/info16030207

[20] Pankratov, E. L. (2011). Optimization of annealing to decrease quantity of radiation defects in a bipolar transistor. *Applied nanoscience*, *1*(3), 123–129. https://doi.org/10.1007/s13204-011-0017-0

[21] Pankratov, E. L., & Bulaeva, E. A. (2012). Decreasing of quantity of radiation defects in an implanted-junction rectifiers by using overlayers. *International journal of Micro-Nano scale transport*, *3*(3), 119-130. https://scispace.com/pdf/decreasing-of-quantity-of-radiation-defects-in-an-implanted-5aax74xf9j.pdf

[22] Fakheri, S., Alimoradi, M., & Yamaghani, M. R. (2024). Colour image multilevel thresholding segmentation using trees social relationship algorithm. *International journal of computer information systems and industrial management applications*, *18*, 34. https://doi.org/10.21203/rs.3.rs-4479475/v1

[23] Pankratov, E. L., & Bulaeva, E. A. (2015). Analytical approach for analysis of mass and heat transport. *Journal of radio electronics*, *9*. http://jre.cplire.ru/koi/sep15/14/abstract_e.html

[24] Carslaw, H. S., & Jaeger, J. C. (1986). *Conduction of heat in solids.* Clarendon Press. https://www.amazon.com/Conduction-Solids-Oxford-Science-Publications/dp/0198533683

[25] Daliri, A., Roudposhti, K. K., Alimoradi, M., Sheikhha, M., Saraei, M. R. S., & Mohammadzadeh, J. (2025). Optimized categorical boosting for gastric cancer classification using heptagonal reinforcement learning and the water optimization algorithm. *2025 7th international conference on pattern recognition and image analysis (IPRIA)* (pp. 1-6). IEEE. https://doi.org/10.1109/IPRIA68579.2025.11263556

[26] Vinetskiy, V. L., & Kholodar', G. A. (1979). *Radiation physics of semiconductors.* Naukova Dumka. (**In Russian**). https://ouci.dntb.gov.ua/works/lx8XpbEl/

[27] Singh, N., Edalatpanah, S. A., & Alimoradi, M. (2025). IoT-driven intelligent traffic systems for congestion management. *Supply chain and operations decision making*, *2*(3), 115–126. https://doi.org/10.48313/scodm.v2i3.37

[28] Fahey, P. M. (1985). *Point defects and dopant diffusion in silicon*. Stanford University.

[29] Landau, L. D., & Lifshitz, E. M. (1986). *Theory of elasticity*. Pergamon Press, Oxford. https://books.google.com/books/about/Theory_of_Elasticity.html?id=tpY-VkwCkAIC

[30] Vorob'ev, A. A., Korablev, V. V, & Karpov, S. Y. (2003). The use of magnesium to dope gallium nitride obtained by molecular-beam epitaxy from activated nitrogen. *Semiconductors*, *37*(7), 838–842. https://doi.org/10.1134/1.1592861

[31] Lamtar Gholipoor, M., Alimoradi, M., & Fakheri, S. (2024). A novel metaheuristic approach inspired by trees social relationships and models for fermentation medium. *Metaheuristic algorithms with applications, 1*(1), 1–11. https://doi.org/10.22105/maa.v1i1.17

[32] Vavilov, V. S., & Ukhin, N. (1977). *Radiation effects in semiconductors and semiconductor devices*. Springer New York, NY. https://www.amazon.com/Radiation-Effects-Semiconductors-Semiconductor-Devices/dp/1468490710

[33] Korn, G. A., & Korn, T. M. (1968). *Mathematical handbook for scientists and engineers: Definitions, theorems, and formulas for reference and review*. McGraw-Hill. https://www.amazon.com/Mathematical-Scientists-Engineers-Definitions-Reference/dp/B0000CO5GE

[34] Pankratov, E. L. (2022). On changing the properties of a multilayer structure by preliminary processing of a substrate. *Computer methods in materials science*, *22*(2), 89–100. https://doi.org/10.7494/cmms.2022.2.0790

[35] Pankratov, E. L. (2022). Influence of missmatch-induced stress and porosity of materials on technological process. *International journal of research in industrial engineering*, *11*(2), 92–118. https://doi.org/10.22105/riej.2022.323547.1279

[36] An, X., Xu, S., Tao, H., Su, H., Yang, H., Xu, K., ... & Hao, Y. (2025). High quality GaN epitaxy induced nucleation by Ar Ion implantation into sapphire substrate. *Journal of inorganic materials*, *40*(1), 91-96. https://doi.org/10.15541/jim20240286

[37] Luu, T. A., Trung, N. V. M., Van, T. N., Turek, M., Drozdziel, A., Pyszniak, K., ... & Hung, N. Q. (2026). Ion implantation-driven defect engineering in BiVO4 thin films for catalytic applications. *Ceramics international*, 52(9), 12572-12588. https://doi.org/10.1016/j.ceramint.2026.01.403

[38] Chalifoux, B. D., Yao, Y., Woller, K. B., Heilmann, R. K., & Schattenburg, M. L. (2019). Compensating film stress in thin silicon substrates using ion implantation. *Optics express*, *27*(8), 11182–11195. https://doi.org/10.1364/OE.27.011182

[39] Pankratov, E. L., & Bulaeva, E. A. (2013). Doping of materials during manufacture p–n-junctions and bipolar transistors. Analytical approaches to model technological approaches and ways of optimization of distributions of dopants. *Reviews in theoretical science*, *1*(1), 58-82. https://doi.org/10.1166/rits.2013.1004

[40] Galib, M., Orhan, O. K., Liu, J., & Ponga, M. (2024). Residual stress development in lattice mismatched epitaxial thin films via atomic and molecular layer depositions. *Journal of the mechanics and physics of solids*, *193*, 105897. https://doi.org/10.1016/j.jmps.2024.105897

[41] Tsai, D. S., Liang, P. Y., Wu, C. Y., Wu, J. R., Chen, C. Y., Chuang, C. M., ... & Kuo, T. C. (2026). Raman mapping analysis of stress and dislocation defect correlation in GaN-on-Si epitaxial layers with and without superlattice structures. *Semiconductor science and technology*, *41*(2), 02LT01. https://doi.org/10.1088/1361-6641/ae4138

[42] Mai, T. T., Dai, J. J., Chiang, C. Y., & Chou, W. C. (2025). Layer-wise dislocation distribution and stress evolution in a GaN-based high electron mobility transistor studied by X-ray nanodiffraction. *ACS applied nano materials*, *8*(30), 15187-15195. https://doi.org/10.1021/acsanm.5c02355

[43] Pankratov, E. L., & Bulaeva, E. A. (2016). On optimization of regimes of epitaxy from gas phase in a horizontal reactor. *Materials science: An Indian journal*, *14*(6), 191-201. https://www.tsijournals.com/articles/on-optimization-of-regimes-of-epitaxy-fromgas-phase-in-a-horizontal-reactor.pdf

[44] Wang, Z., Wang, S., Liu, L., Yu, J., Wang, G., Li, Q., ... & Zhang, L. (2024). Growth of freestanding GaN crystals on three-dimensional mesh porous substrates by HVPE. *CrystEngComm*, *26*(38), 5415-5420. https://doi.org/10.1039/d4ce00726c